Electrochemical Corrosion Failure Analysis of Large Complex Engineering Structures by using μ LPR Sensors

M. H. Nazir [1], A. Saeed [2], Z. A. Khan[1]

[1]Bournemouth University
NanoCorr, Energy and Modelling Research Group (NCEM)
Faculty of Science and Technology, Bournemouth, UK

[2] Global College of Engineering and Technology
P.O.Box 2546, CPO Ruwi 112,
Muscat Sultanate Oman

Abstract

This paper presents the effects of three major parameters; temperature, relative humidity and hygroscopic salts contaminants on the atmospheric corrosion of large steel structures. The effects of these three parameters have been analysed by using micro-sized LPR sensors to continuously monitor the corrosion rate of a degrading large structure under varying parameters. A long term, three years study was performed by deploying μ LPRs on strategically selected large military vehicles (main battlefield tanks), which are stationed in the Tank Museum at Bovington, UK. These vehicles are operational and are of historic significance with cultural biography, however structural deterioration through corrosion, corrosion fatigue, stress corrosion cracking and mechanical failures are a threat to these vehicles in terms of their conservation. A set of vehicles operational (uncontrolled environment) and non-operational (controlled environment) was selected for comparative analysis in context of corrosion rate. This research is founded on a novel real-time corrosion monitoring technique that enables to better understand the relationship between varying environmental parameters and corrosion rate of large steel-based mobile structures during operation. This research provides a synthesis of real time corrosion data, which has been accumulated over a period of three years. An overview of structural deterioration is presented and derived from a significantly large data, therefore it provides a more reliable and highly accurate assessment of failures due to corrosion.

Keywords: Steel structures; Atmospheric corrosion; Corrosion sensors; Relative humidity; High value assets

Table of Contents

1. Introduction

The most important factor in atmospheric corrosion is moisture, either in the form of high relative humidity (RH) or condensate on the surface of metal substrate. The maximum amount of moisture the atmosphere can hold increases as the temperature increases [1]. When the atmosphere cannot hold all the moisture, then it condenses forming a thin electrolytic layer on steel substrate. This thin layer along with pre-existing corrosive contaminants deposits on the surface of steel such as hygroscopic salts forming a high alkaline electrolytic solution which accelerates the corrosion rate [2]. While thin film is almost invisible, the corrosive contaminants it contains are known to reach relatively high concentration, especially under operating conditions of structures (such as vehicles) in outdoor open atmosphere and places near to coastal regions.

When steel surfaces become contaminated their surface can be wetted at lower relative humidity therefore, reducing the critical relative humidity of steel. The critical relative humidity of steel is a variable term that depends on the nature of the corroding material, the atmospheric temperature, the atmospheric contaminants and the tendency of surface contaminants to absorb moisture. For example the critical relative humidity of steel is in the region of 60 - 65% if the surface is contaminated with particles of sodium chloride, or ammonium sulphate, or if the atmosphere contains sulphur dioxide. However in the absence of strong electrolytes the critical relative humidity value of steel remains high such that in some cases, even at 100% relative humidity, the corrosion rate remains fairly low [3].

Lower critical humidity accounts for early initiation of corrosion at low relative humidity values due to high wettability rate of steel [4]. Therefore wettability of steel is an important parameter in deciding the corrosion rate. The wettability is measured in terms of time of wetness (TOW) [4] which is a complex parameter and in addition to critical relative humidity also depends on many other physical parameters such as type of surface, surface roughness, position and orientation of exposed surface and frequency of exposure. Therefore, undoubtedly it can be said that atmospheric corrosion rate of steel is a function of its compositional characteristics, relative humidity, temperature, hygroscopic salts contaminants, critical relative humidity of steel and TOW as shown in fig. 1. Understanding the comprehensive relationship between corrosion rate and these parameters is of vital importance for controlling the detoriation of steel based large structures. This research is an effort in understanding this complex relationship.

In this paper, the study of the corrosion of large steel structures will revolve around the effects of three major parameters: temperature, relative humidity and contaminants. Although, significant in-situ laboratory analyses of corrosion degradation of steel already exists in literature but continuous real time corrosion monitoring of large steel-based operating structures corresponding to the above changing parameters is still an area which needs further research. This latest approach of continuous corrosion monitoring of structures by using high-tech micro-sized LPR sensors advantages in data/information collection and analysis based on ‘when and where needed’. Further it helps in analysing ‘not-easily-accessible sites’ on complex engineering structures.

Previous investigation of coating failures, i.e. blistering, delamination, micro-cracks and corrosion damage measurement in real time has been reported [5-28]. This research focuses on analysing the corrosion failure of large military vehicles (battle tanks) corresponding to changing relative humidity, temperature and concentration of surface contaminants by using μ LPR sensors. These vehicles consisting of a fleet of three hundred battle tanks are situated at the Tank museum, Bovington UK. The vehicles are of historical importance however corrosion is one of the most significant contributors to the structural damage and material aging of these large vehicles. Therefore, corrosion monitoring technique was utilised to monitor the continuous degradation of vehicles. For this, two set of vehicles (operating and stationary) were selected for a long term experiment,

comprising of three years (Aug. 2013 to Aug. 2016) comparative analysis. A comparative study between the results of two set of vehicles was performed to understand the relationship of varying environmental parameters with the corrosion rate under the operational conditions. The experiment helped in understanding the prevailing mechanisms of failures due to corrosion with various types occurring in these vehicles identified.

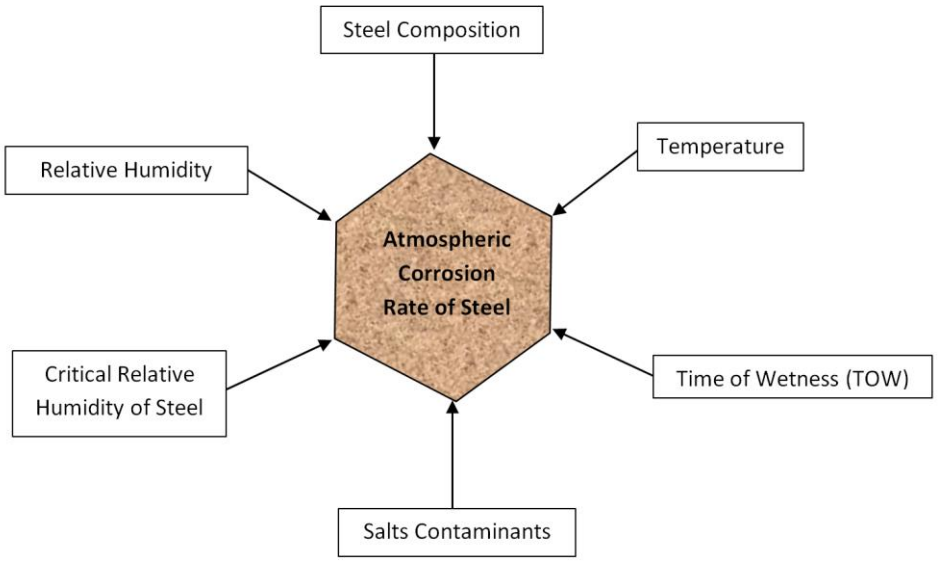

Figure 1. Figure showing that atmospheric corrosion rate of steel is a function of its compositional characteristics, relative humidity, temperature, hygroscopic salts contaminants, critical relative humidity of steel and TOW

2. μ LPR

LPR (Linear Polarization Resistance) monitoring is an effective electrochemical method of measuring corrosion. Monitoring the relationship between electrochemical potential and current generated between electrically charged electrodes in a process stream allows the calculation of the corrosion rate. This measurement of the actual corrosion rate allows almost instant feedback to operators [29].

A two or three electrode probe is inserted into the process system, with the electrodes being electrically isolated from each other and the process line. A small potential in the range (in mV's which does not affect the natural corrosion process), is applied between the elements and the resulting current is measured. The polarization resistance is the ratio of the applied potential and the resulting current level. The measured resistance is inversely related to the corrosion rate. The electrical resistance of any conductor is given by: R = V/ I. Where R = Effective instantaneous resistance V = Applied voltage and I = Instantaneous current between electrodes. If the electrodes are corroding at a high rate with the metal ions passing easily into solution, a small potential applied between the electrodes will produce a high current, and therefore a low polarization resistance. This corresponds to a high corrosion rate [29].

Recently, Analatom's developed commercially available, μ LPR [30-36] is the micro-scaled small form factor of conventional LPR measurement setup [37, 38] which is designed to minimize the volume of an electrochemical corrosion monitoring setup as shown in fig. 2 (a). μ LPR sensor can be used for corrosion monitoring of variety of steel based industrial applications [36] to aluminium based aerospace applications [31].

μ LPR has dimensions 40 mm x 20 mm x 0.1 mm. The sensor consists of multiple plates made from the material of interest which form the two electrodes (counter and reference). The electrodes are used in conjunction with a potentiostat for conducting LPR measurements. The use of relatively large counter electrode minimizes polarization effects at the counter electrode to ensure that a stable reference potential is maintained throughout the experiments. Potential step-sweeps are performed by applying a series of 30 steps over a range of ±10 mV spanning a period of 2.6 s [39]. μ LPR measures the polarization resistance $R_p(\Omega)$ between the corrosive agents

(electrolytic solution) and the steel substrate. The polarization resistance is then used to calculate the corrosion current density '*i*' and subsequently corrosion rate of steel structure [40],

The μ LPR is adhered to the conditioned face of the steel samples with industrial strength epoxy as shown in fig. 2 (b). The sensor array includes at least two interlaced inert electrodes which are manufactured of a noble metal. The noble metal could be Au, Pt and Pd because of the low contact resistances. The noble metals are principally inert such that the sensor array does not readily corrode in typical ambient environments.

The μ LPR is connected to data acquisition unit (DAQ) which is able to connect up to eight μ LPRs in addition to relative humidity and temperature sensors as shown in fig. 2 (c). The relative humidity and temperature sensors monitor the humidity and temperature levels corresponding to corrosion rate data samples. Salinity is measured by using the resistance (or conductivity) measured between the two interdigitated μ LPR electrodes by using method detailed in [41]. Data can be retrieved by using a RS232 wired interface. The software converts LPR and resistance data into a corrosion rate. This unit is internally powered by a 3.6 V lithium thionyl chloride cell battery, which provides monitoring lifetime of 5-7 years depending on duty cycle and temperature conditions.

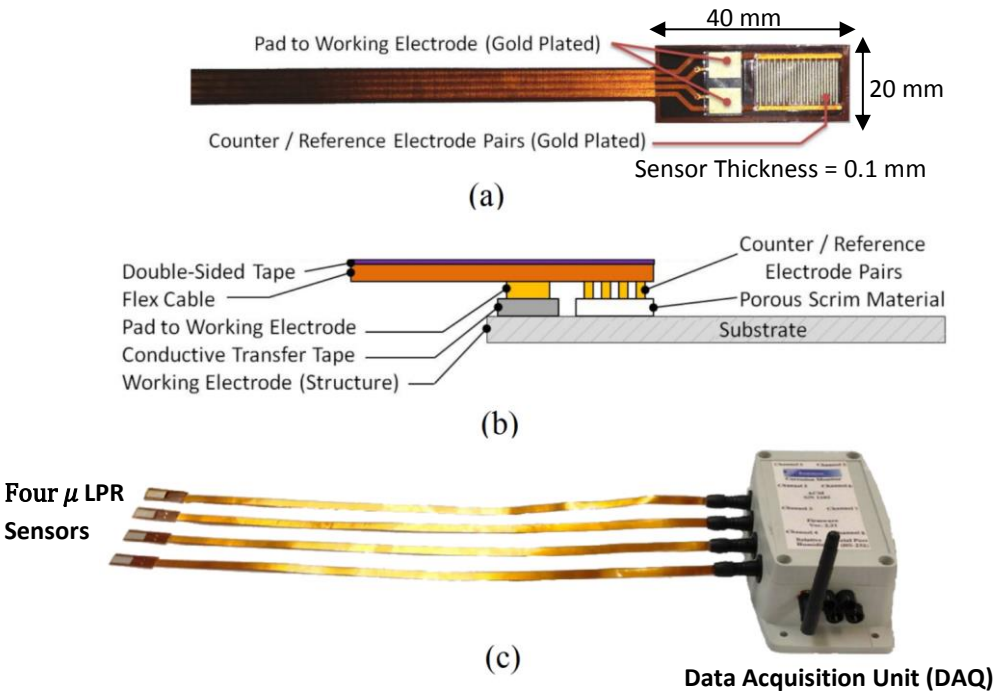

Figure 2. (a) Schematic of a μ LPR corrosion sensor (b) installed on substrate and (c) a group of 4 μ LPR sensors connected to DAQ [41]

3. Research Problems

1) To understand complex relationship between the varying environmental parameters: temperature, relative humidity, hygroscopic salts contaminants and the corrosion rate of large steel based structures such that the structure is being operated under uncontrolled environmental conditions.
2) The application of μ LPR based real-time corrosion monitoring technique for understanding the above complex relationship.

4. Experiment

4.1. Setup

Two set of vehicles were used for experimental analysis, stationary set (fig. 3 (a)) and an operating set (fig. 3 (b)) at the Tank museum. Operating set included a group of two vehicles in constant operation under uncontrolled environmental conditions while stationary set included another group of two vehicles permanently preserved inside the Tank Museum under controlled conditions. The two operating vehicles were operated at the same time and under the same uncontrolled environmental conditions. The reason for setting two vehicles in each set (operating and stationary) was to ensure the repeatability. A three years study (Aug. 2013 to Aug. 2016) was performed on these two set of vehicles. The study included the collection of data from μ LPR sensors, taken from both stationary and operating set. The operating set was used 8 times (known as operations A, B, C, D, E, F, G and H) in round trips (in-and-out) during three years. While the stationary set was preserved inside the museum. All eight operations were performed during the summer time in April, May and June of every year in sequence mentioned in Table 1. Operation A was performed in April 2014, operation B was performed in May 2014. Similarly at the end of study, operation H was performed in May 2016.

Each round trip (operation) of the operating set was for a duration of 5 days continuous exposure to outdoor conditions, meaning that these vehicles were fully operated outdoor during these five days and returned to the controlled environment (inside shed) at the end of fifth day. Every vehicle of the operating set was installed with eight µ LPR sensors. Similarly every vehicle of the stationary set was installed with eight µ LPR sensors. These sensors were installed for the duration of three years in order to constantly monitor corrosion rate for making comparative corrosion rate analysis of both the sets. All the sensors were connected to the corresponding ports of DAQ through wires as identified in fig. 4. The data sampling rate was set as one sample collection from all sensors after every 15 minutes.

Table 1. Operations performed in various seasons

Operations	Annual Season
A	April 2014
B	May 2014
C	June 2014
D	April 2015
E	May 2015
F	June 2015
G	April 2016
H	May 2016

The eight sensors were installed on exposed metal parts of vehicles i.e. bare steel. Six inside sensors, including µ LPR3 and µ LPR 4 were installed on uncoated parts of the gun barrel while other sensors µ LPR5, µ LPR6, µ LPR, 7 and µ LPR8 were installed on inner vertical walls of hull where coating has already delaminated due to corrosion, as can be seen in fig. 5. Similarly two outside sensors µ LPR1 and µ LPR2 were installed on delaminated area of turret top. Before installing sensors, the steel surface was pre-treated with the solution of 50 g/L Turco 4215 NC-LT in order to remove any pre-existing contaminants. After cleaning, each sensor was installed.

Both the operating and stationary sets of vehicles were made up of same material (steel AISI-1010) and had similar dimensions, both inside and outside. Both sets were painted at same time with same coating type and under same conditions. Inside the Tank museum (controlled environment), the temperature is kept between (18 - 25°C) and RH maintained at 40% throughout the year. However, outside (uncontrolled environment) temperature can go as low as 0^{o}C during winter and as high as 30^{o}C during summer. Museum is located approximately 9km north of the Atlantic Ocean/English channel as shown in fig. 3 (c). There is significant precipitation in this area, where fog, rain, and/or snow are reported, on average, for 18 days of each month [42].

Figure 3. (a) A stationary large vehicle (preserved) from the stationary set (b) An operating large vehicle from the operating set (c) Location of the Tank Museum [43]

Figure 4. μ LPR sensors installed at various locations inside the tank. The last two images show the data acquisition unit (left) and PC connected to data acquisition unit to retrieve the data.

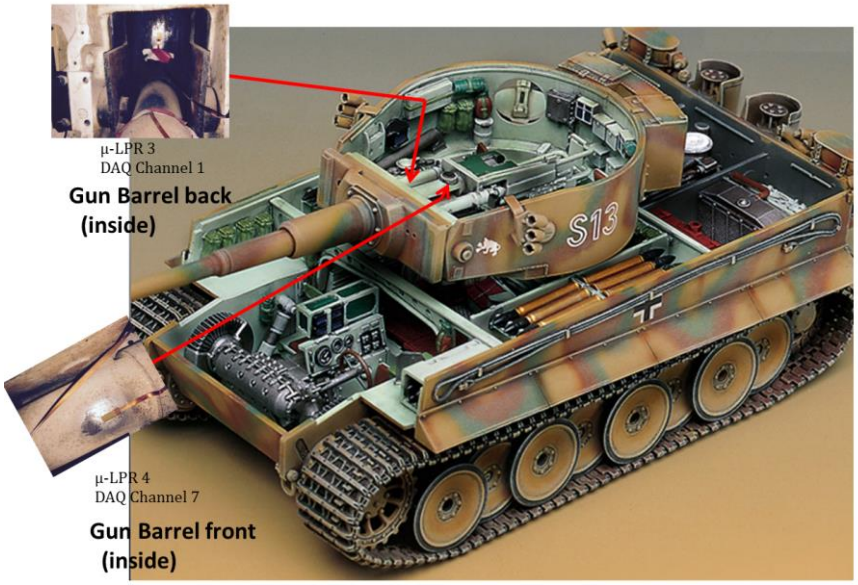

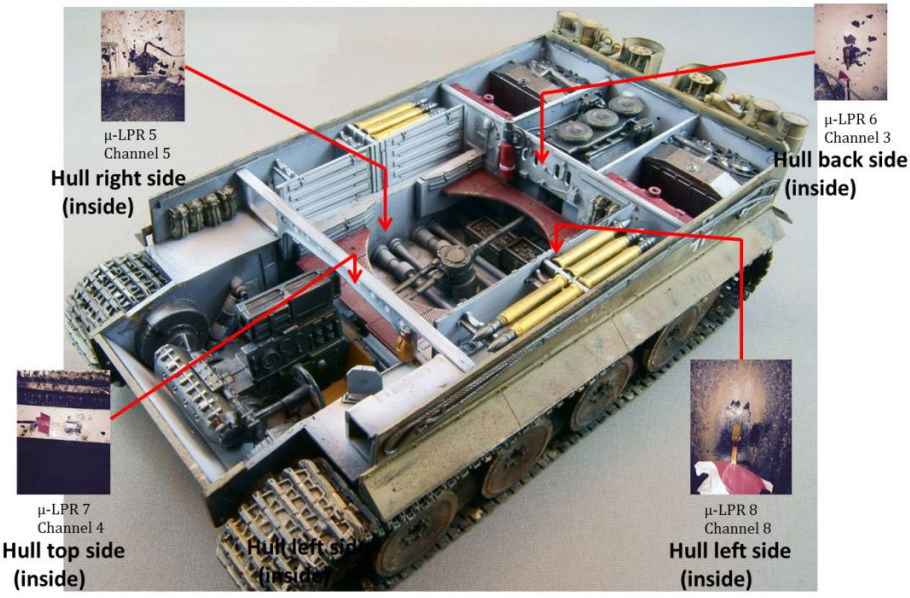

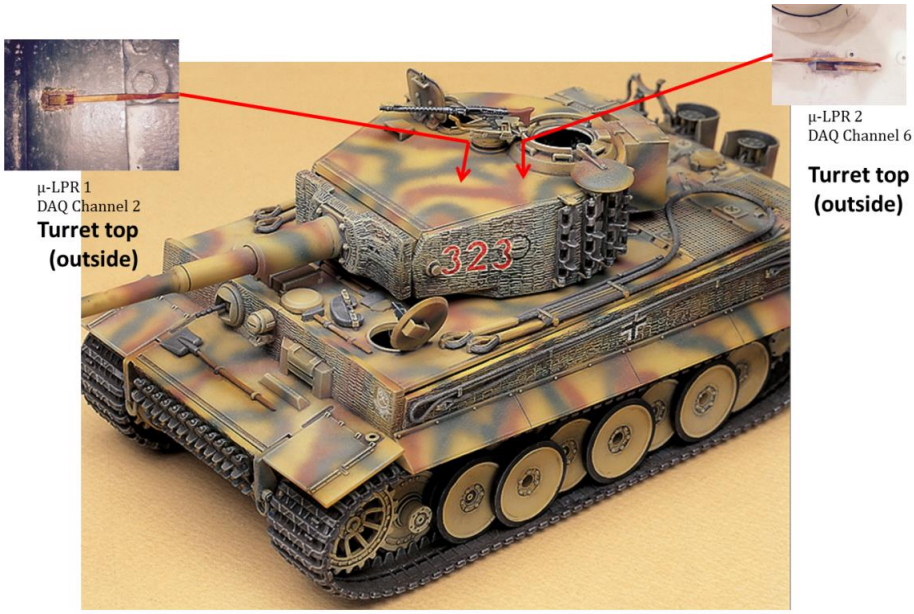

Figure 5. Figures showing location of eight μ LPR corrosion sensors installed at various locations on each the large vehicle. μ LPR1 and μ LPR2 were installed on the turret top (Top figure); μ LPR3 and μ LPR4 were installed on the gun barrel (Middle figure); μ LPR5, μ LPR6, μ LPR7, μ LPR8 were installed inside the hull (Last figure). Images of battle tanks have been taken from [44]

4.2. Experimental Results and Discussion

In this section, the experimental results of three year long-term experimental analysis are presented. For simplicity and for the sake of discussion, the data from only one vehicle from each set has been presented. These two vehicles from each set are termed as 'operating vehicle' and 'stationary vehicle' respectively.

4.2.1. Results from an operating vehicle

A. Temperature, Relative Humidity and Salinity data

Fig. 6 shows the time (at top) and data samples (at bottom) of the temperature, relative humidity and salinity from field exposure test of an operating vehicle measured at the Tank museum site for three years. A total of 100,000 corrosion data points were collected for constant ~3 years/1000 days.

In fig. 6, the spike A (along the green line) shows that the lowest temperature value (T_L = 6^{o}C) accounts for the highest relative humidity value (RH_H = 81%) where 'L' and 'H' in subscript denote the lowest and highest values. Similarly all other temperature spikes and their corresponding humidity spikes show similar corelation and are denoted as B, C, D, E, F, G and H in figure. It should be noted that each spike represents the operation of vehicle (A to H) from controlled environment (inside shed) to uncontrolled environment (outside shed) for example during operation A (along green line), when the vehicle was operated from controlled to uncontrolled environment, the relative humidity increased from 30% to 81% due to corresponding decrease in controlled temperature from 21^{o}C to 6^{o}C.

Correspondingly, during this operation A, the salinity value of condensate varied significantly as shown in the bottom graph of fig. 6. The operation of vehicle in uncontrolled environment resulted in the contamination of unprotected steel surface due to accumulation of hygroscopic salts. As the Tank Museum is located near coastal region, therefore each movement of vehicle from controlled to uncontrolled environment resulted in salts being accumulated on unprotected steel parts. When the vehicle is outside under uncontrolled conditions, the temperature is low while relative humidity is high which provides adequate electrolytic medium for the

formation of saline solution in the presence of hygroscopic salts which therefore results in high salinity. For example it can be seen along the green line that during uncontrolled movement, as the temperature drops from 21°C to 6°C and relative humidity increase from 30% to 81%, the corresponding salinity increases from 0 g/L to 38 g/L. In the case when the vehicle returns back to controlled environment after a round trip, the accumulated salts settle down on the surface of steel after the evaporation of condensate. As the electrolyte evaporates leaving behind salts, the salinity level again drops back to zero. This accumulation of salts greatly reduces the critical relative humidity level of vehicle's steel which means that steel can be wetted at lower relative humidity level resulting in early initiation of corrosion. The critical relative humidity is a threshold humidity value after which the metal begins to absorb moisture from the atmosphere and below which it does not absorb atmospheric moisture. Critical relative humidity is a function of vapour pressure, temperature and salinity unlike relative humidity which is only a function of vapour pressure and temperature such as,

$$\textbf{Critical relative humidity}\ (\%) = \textbf{function}\ [\textbf{Vapour pressure};\ \textbf{Temperature};\ \textbf{Salinity}] \quad (1)$$

In eq. 1, the salinity value of condensate decides the particular critical relative humidity point. For constant temperature and vapour pressure, higher condensate's salinity accounts for lower critical relative humidity and vice versa.

The wettability of steel due to lower critical relative humidity becomes a serious problem for operating vehicle because the vehicle is historic and paint is torn and worn at most of its steel parts exposing them to environment. The time period after which the relative humidity exceeds the critical relative humidity point for the formation of a surface layer of moisture on steel surface is called as Time of Wetness (TOW). This is a complex variable, since TOW includes many other physical parameters in addition to critical relative humidity as shown in eq. 2,

$$\text{TOW (hours)} = \text{function}\ [\text{critical relative humidity};\ \text{type of surface, surface roughness, position and orientation of exposed } \textbf{surface};\ \textbf{frequency of operation of vehicle}] \quad (2)$$

The TOW of a corroding steel is a key parameter, directly determining the duration of the corrosion reactions because TOW decides the period for which the steel surface will remain wet for reactions. Therefore eq. 3 shows that,

$$\textbf{Corrosion rate}\ \left(\frac{\textbf{mg}}{\textbf{cm}^2}\right) = \textbf{function}\ [\textbf{Time of Wetness}\ (\textbf{TOW})] \quad (3)$$

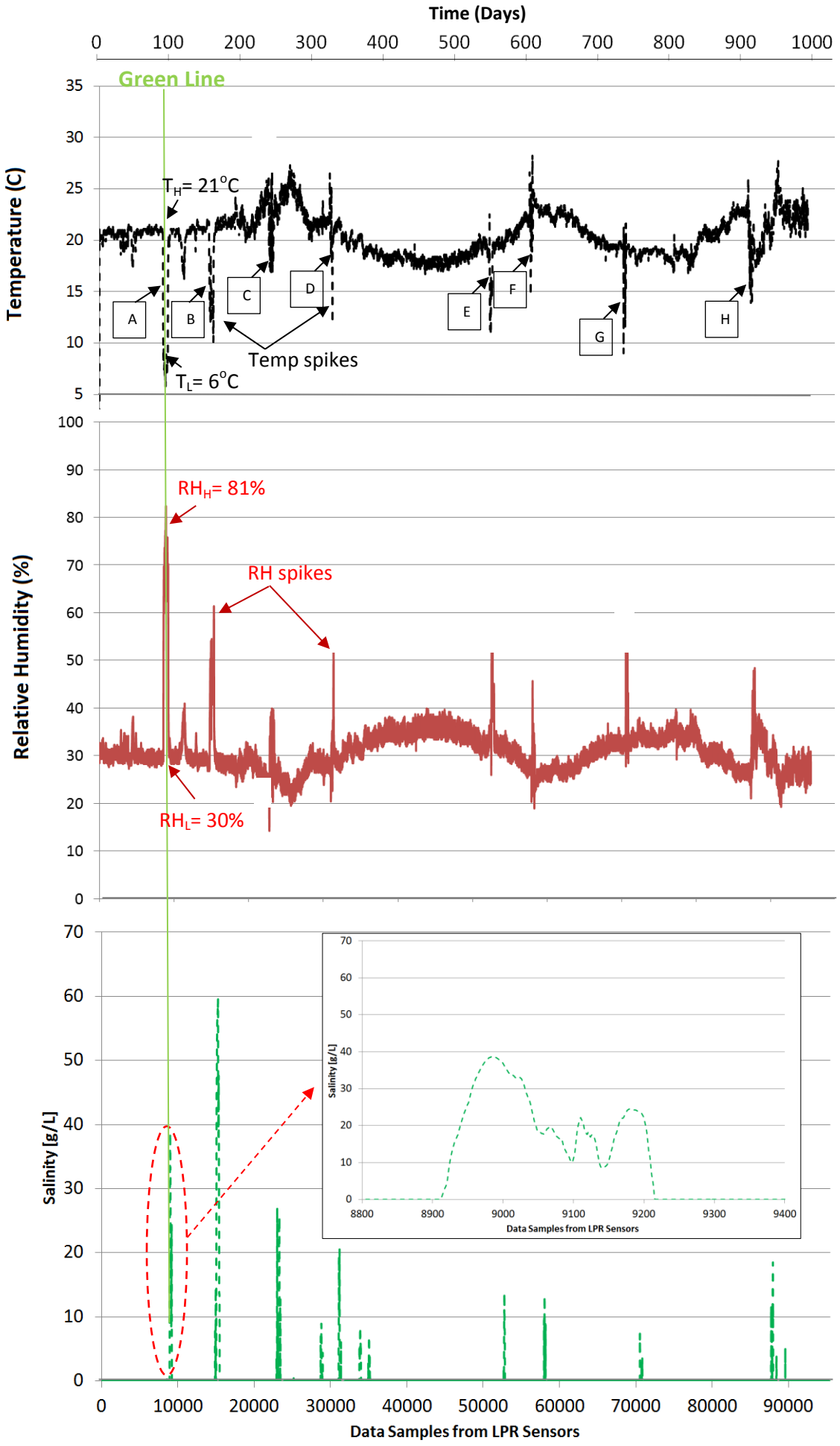
Time (Days)
0 100 200 300 400 500 600 700 800 900 1000
Green Line
Temperature (C)
35 30 25 20 15 10 5
T_H= 21°C
T_L= 6°C
A
B
C
D
E
F
G
H
Temp spikes
Relative Humidity (%)
100 90 80 70 60 50 40 30 20 10 0
RH_H= 81%
RH spikes
RH_L= 30%
Salinity [g/L]
70 60 50 40 30 20 10 0
0 10000 20000 30000 40000 50000 60000 70000 80000 90000
Data Samples from LPR Sensors
Salinity [g/L]
70 60 50 40 30 20 10 0
8800 8900 9000 9100 9200 9300 9400
Data Samples from LPR Sensors

1

Figure 6. Figure sshowing the data samples of the temperature, relative humidity and salinity in a field exposure test of an operating vehicle measured in the Tank museum site for three years

B. Corrosion rate data

The long-term three years atmospheric corrosion rate data corresponding to the changing temperature, relative humidity and condensate's salinity is shown in fig. 7. Since the values of temperature, relative humidity and salinity in fig. 6 changed drastically due to operations A to H from controlled to uncontrolled environment over the three years duration, the corresponding corrosion rate also changed significantly which was monitored by eight µ LPR sensors.

It can be seen from fig. 7 and fig. 8 (a) that during operation A of vehicle to uncontrolled environment, the corrosion rate of four µ LPR sensors (µ LPR1, μ LPR2, μ LPR3, μ LPR4) installed at various locations on vehicle detected corrosion corresponding to decrease in temperature, increase in relative humidity and increase in average salinity. The period during which sensors detected corrosion is highlighted with transparent 'yellow' colour in fig. 8 (a). It is during this period, when moisture condensed on unprotected steel forming high salinity thin electrolytic layer. It is worth noting that during operation A, the critical relative humidity level was low i.e. 62%. This means that only 62% of relative humidity (much lower than 100%) was sufficient for condensation of moisture which initiated the surface corrosion detected by μ LPR sensors as shown in Table 1. Table 1 shows the type and number of sensors which detect corrosion. The reason for low critical relative humidity was already presence of hygroscopic salts on unprotected steel areas which resulted in early initiation of corrosion and high TOW. Pre-TOW is the time during which the metal is not sufficiently wet for the corrosion to start. However as soon as the metal attains a sufficient degree of wetness, at critical humidity point the corrosion initiates, as detected by µLPR sensors in fig. 8 (a).

The graphs for corrosion rates during operation B is shown in fig. 8 (b). It can be seen that in addition to μ LPR1, μ LPR2, μ LPR3 and μ LPR4 (in the case of operation A), now two more sensors µ LPR6 and µ LPR7 installed inside at the hull walls, started to detect corrosion rate. As humidity exceeded the critical relative humidity level equal to 34%, corrosion rate for all sensors increased with subsequent decrease when humidity became less than critical relative humidity.

Similar to operation A and B, the graphs of corrosion rates for further operations C, D, E, F, G and H during three years period are shown in Table 3 respectively. All eight operations follow similar correlation between corrosion rate, temperature, relative humidity and salinity as in case of A and B, therefore corresponding correlation for each operation C, D, E, F, G and H can be understood from the presented graphs in Table 3.

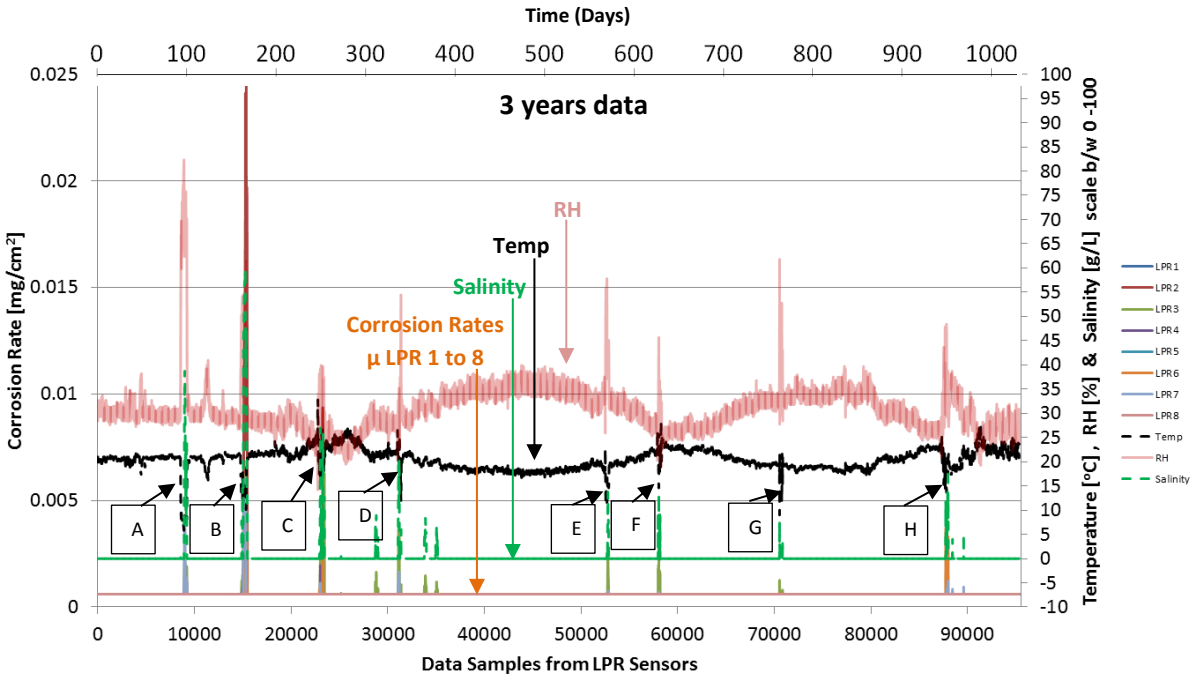

Figure 7. The long-term three years atmospheric corrosion rate data from operating vehicle corresponding to the change of temperature, relative humidity and condensate's salinity

Table 2. μ LPR corrosion Sensors which are detecting corrosion corresponding to each operation

Operations	μ LPR Corrosion Sensors Detecting Corrosion	Number of μ LPRs Detecting Corrosion
Operation A	μ LPR1, μ LPR2 (Horizontal Turret Top) μ LPR3, μ LPR4 (Horizontal Gun Barrel)	4
Operation B	μ LPR1, μ LPR2 (Horizontal Turret Top) μ LPR3, μ LPR4 (Horizontal Gun Barrel) μ LPR6, μ LPR7 (Vertical Hull walls)	6
Operation C	μ LPR1, μ LPR2(Horizontal Turret Top) μ LPR3, μ LPR4 (Horizontal Gun Barrel) μ LPR6, μ LPR7 (Vertical Hull walls)	6
Operation D	μ LPR1 (Horizontal Turret Top) μ LPR3 (Horizontal Gun Barrel)	2
Operation E	μ LPR1 (Horizontal Turret Top) μ LPR3 (Horizontal Gun Barrel)	2
Operation F	μ LPR1 (Horizontal Turret Top) μ LPR3 (Horizontal Gun Barrel)	2
Operation G	μ LPR3 (Horizontal Gun Barrel)	1
Operation H	μ LPR1 (Horizontal Turret Top)	1

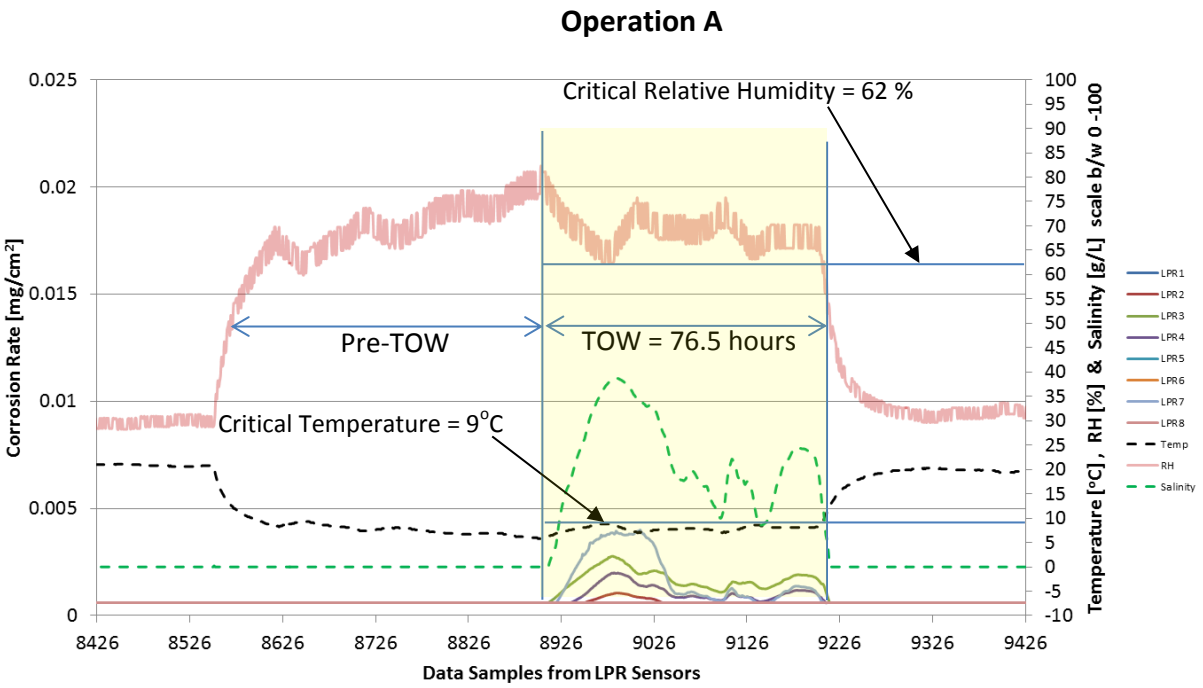

(a)

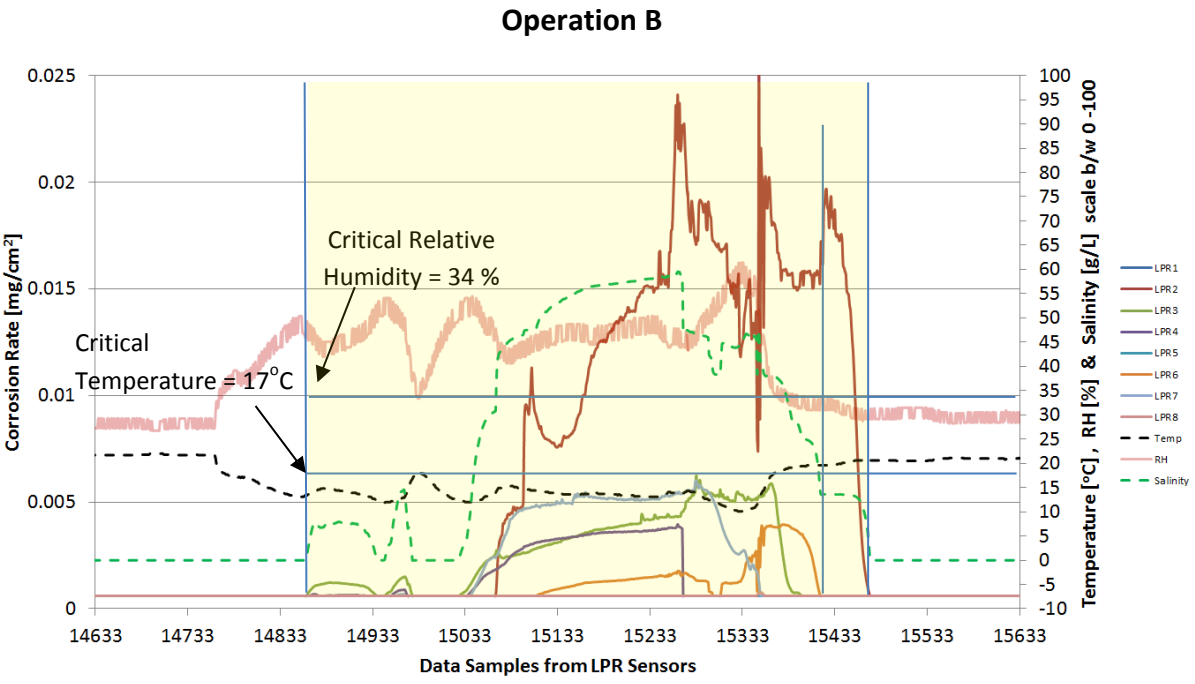

(b)

Figure 8. Graphical data for each opeartion shown in fig. 8(a) operation A (b) operation B

Table 3. Graphical data for operations C,D, E, F, G and H

Operation C	Operation D	Operation E
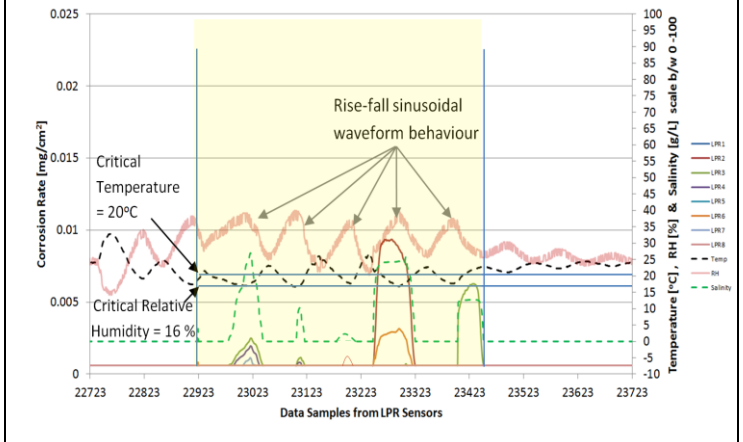	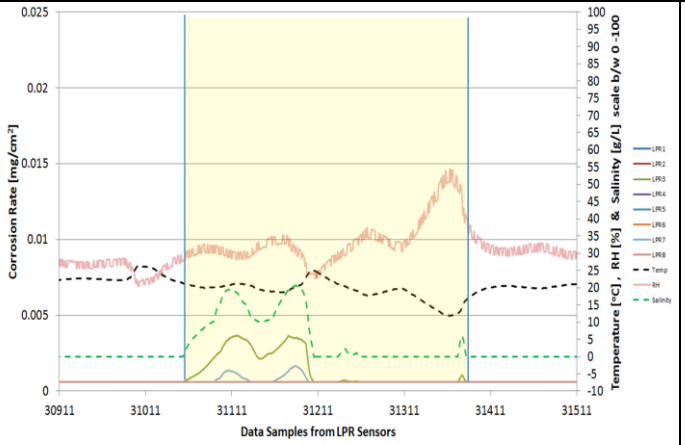	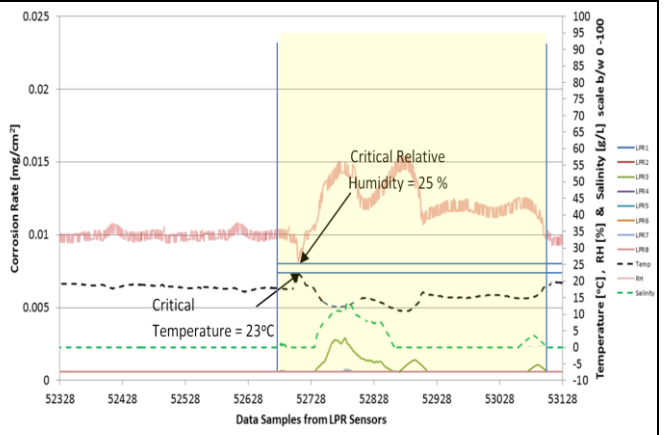
Operation F	**Operation G**	**Operation H**
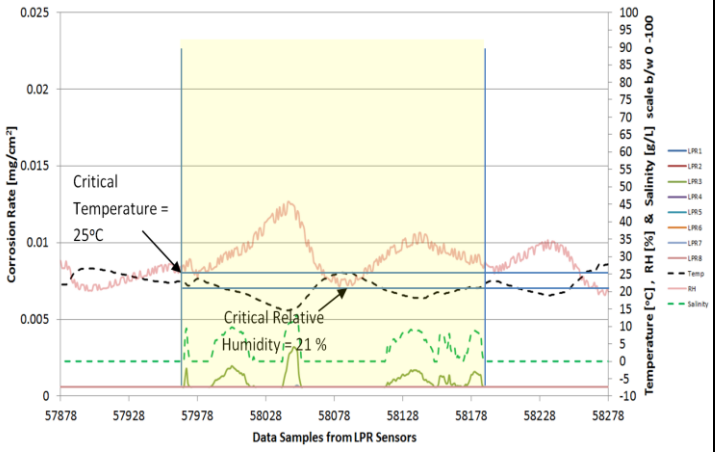	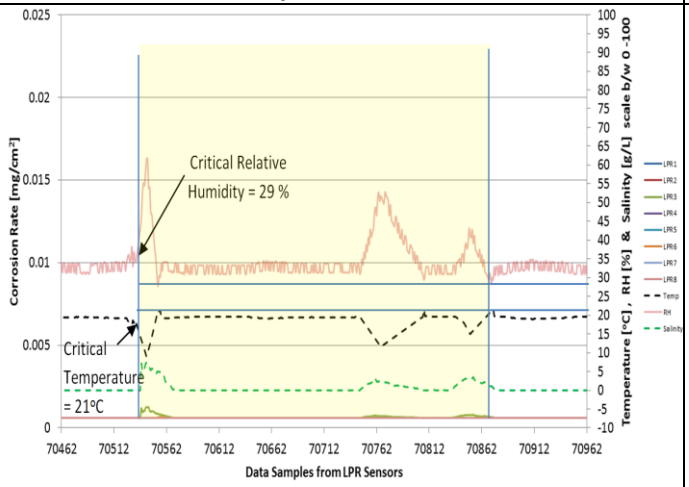	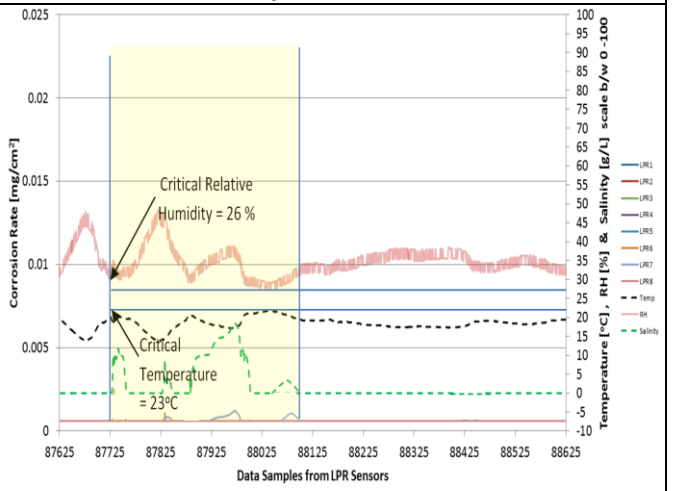

1

Critical value is important in a sense that it identifies the failing point. Here, critical relative humidity, critical temperature and TOW values for each operation are plotted in fig. 9. It can be seen that during the first operation A the critical relative humidity of steel is 62% and the corresponding critical temperature and TOW are 9°C and 72 hours respectively. After first outdoor round trip A, the steel surface becomes more contaminated, and therefore during operation B, the critical relative humidity becomes further low (34%) and the corresponding TOW (162.5 hours) become high. This means that the surface contaminants help in absorbing moisture from air which reduces the critical relative humidity level and sets a low threshold for the moisture to start forming on metal surface therefore increasing TOW. In the subsequent operation C, the metal surface has become even more contaminated which further reduces the critical relative humidity level to 20%. However, here an interesting point is that although the critical relative humidity has significantly decreased allowing the formation of moisture at reduced threshold point but this time TOW reduces (132 hours) rather than expected increase. The possible reason is that the metal surface has started developing a thin layer of corrosion product which hinders the fresh diffusing contaminants reaching the bare metal surface thus passivating the metal and reducing TOW. After operation C, all the parameters including critical relative humidity, critical temperature and TOW become stable with the formation of thick layer of corrosion product as can be seen from fig. 9.

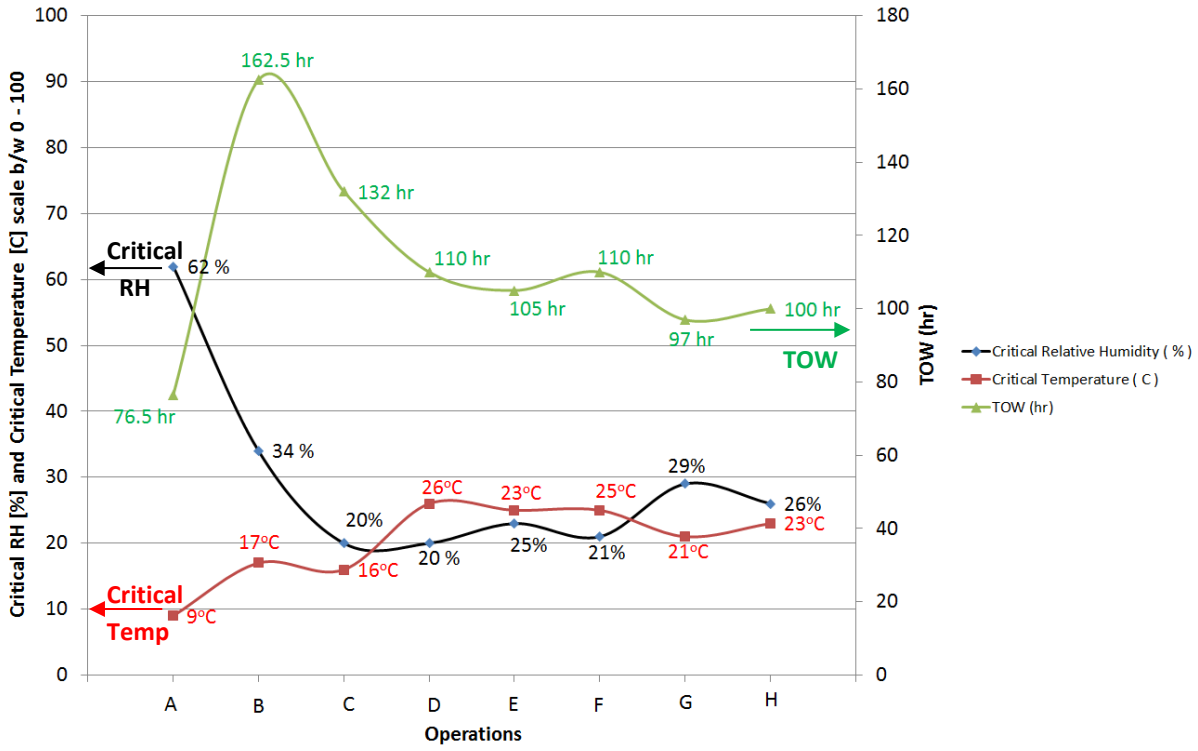

Figure 9. Figure showing the trends for critical relative humidity, critical temperature and TOW as a function of all operations starting from from the first operations A to the last operation H

The average corrosion rate for all eight sensors during each operation is plotted in fig. 10. As evident from eq. 3 that the corrosion rate is a direct function of TOW, therefore it can be seen that initially during operation A corrosion rate is low (9.43 e^{-04} mg/cm^2) because TOW is low i.e. 72 hours, as can be seen from fig. 9. However, with the increase in TOW to 162.5 hours, the average corrosion rate also increases (2.33 e^{-03} mg/cm^2) during operation B. In the next operation C, the TOW reduces to 132 hours due to the formation of a thin layer of corrosion product which results in the decrease in average corrosion rate (8.56 e^{-04} mg/cm^2). After operation C, the average corrosion rate for the rest of operations (D, E, F, G and H) becomes constant because of almost stable value of TOW (± 10 hours).

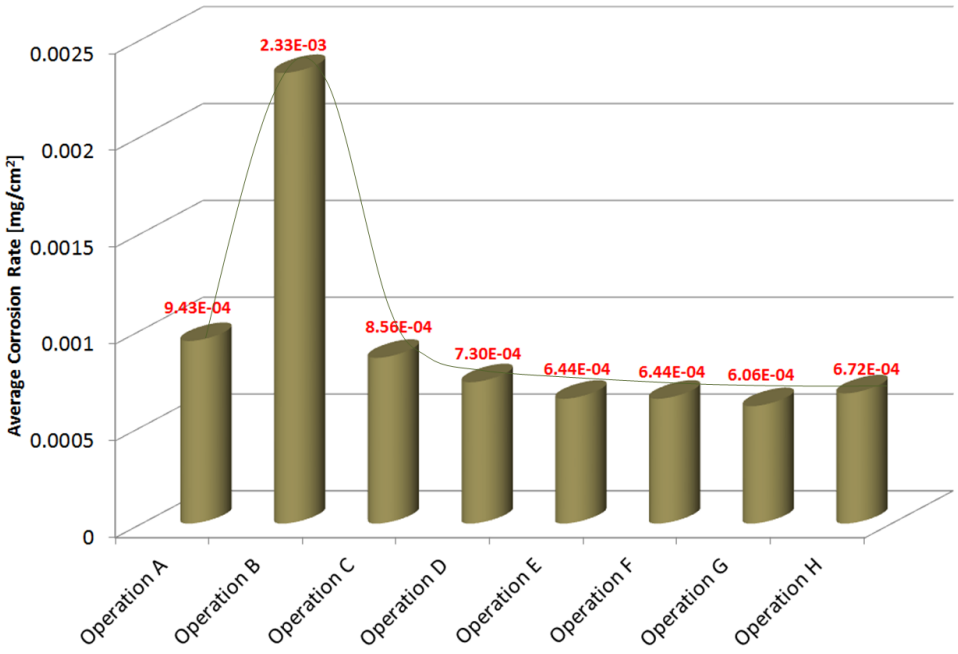

Figure 10. The average corrosion rate for all eight μ LPR sensors during each operation

For the purpose of repeatability, the three years atmospheric corrosion rate data of another operating vehicle in an operating set is shown in fig. 11. As the two operating vehicles in the operating set were operated at the same time and under the same environmental conditions therefore it can be seen that the overall trends for the corrosion rate from all the µ LPR sensors in operating vehicle 2 were almost similar to the other operating vehicle (discussed previously in fig. 7). It can be seen that initially during operation A, the corrosion rate is low which subsequently increases during operation B and then becomes constant for the rest of operations.

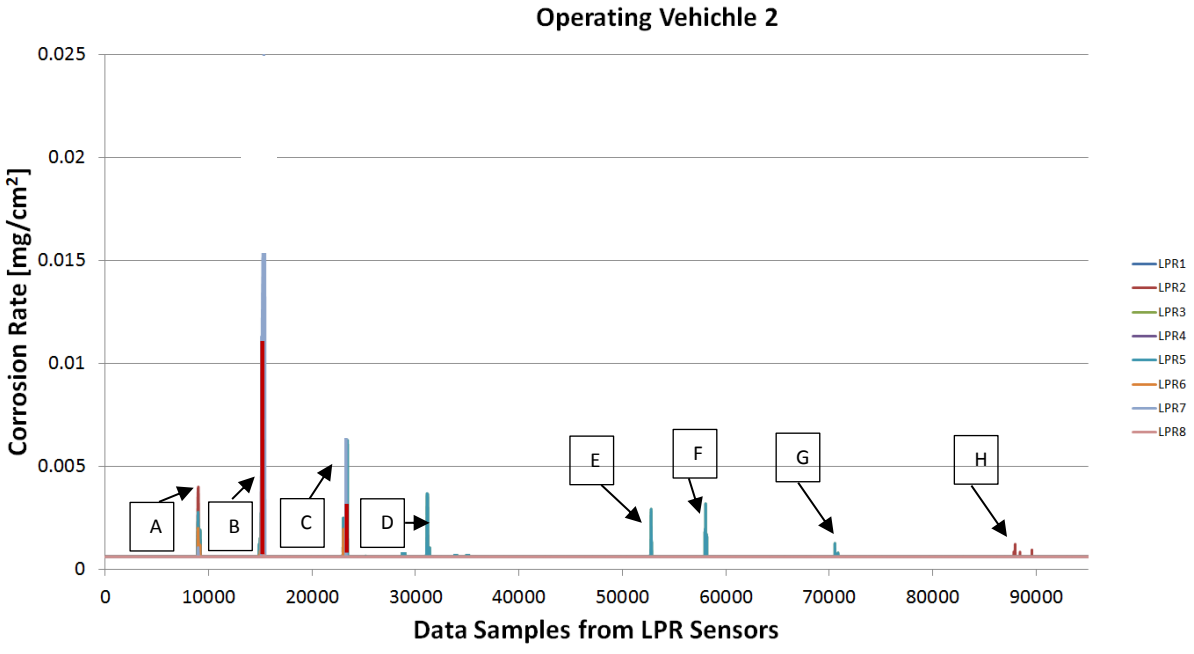

Figure 11. The corrosion rate data for the operating vehicle 2. This vehicle was operated under the same environmental conditions and at the same time as other operating vehicle (discussed previously) in the operating set in order to ensure the repeatability. The results obtained from operating vehicle are almost similar to the other vehicle

4.2.2. Results from a stationary vehicle

It can be seen from fig. 12 that during the three years of data collection from stationary vehicle, the eight µ LPR sensors installed at various locations on vehicle did not show any reading. The reason is that this vehicle was permanently preserved inside the museum, where no significant changes in temperature, relative humidity and salinity values were observed in the form of spikes (A to H), as in the case of operating vehicle. Although the normal RH and temperature inside the museum is maintained at 30% and 21°C, however in reality they both can incur a variation of ±20. It can be seen that maximum and minimum variation in relative humidity throughout three years inside the museum was between RH_H = 47% and RH_L = 17% respectively. Though, 47% relative humidity is high enough to initiate the corrosion at low critical relative humidity condition of steel, but as the vehicle was permanently preserved inside the museum, therefore no hygroscopic salt impurities were accumulated on its surface which resulted in high critical relative humidity, far greater than 47 % (close to or equal to 100 %). Due to this high critical relative humidity, no corrosion was observed throughout the three year of experimental study. Stationary vehicle 2 similar to the stationary vehicle 1 did not show any corrosion.

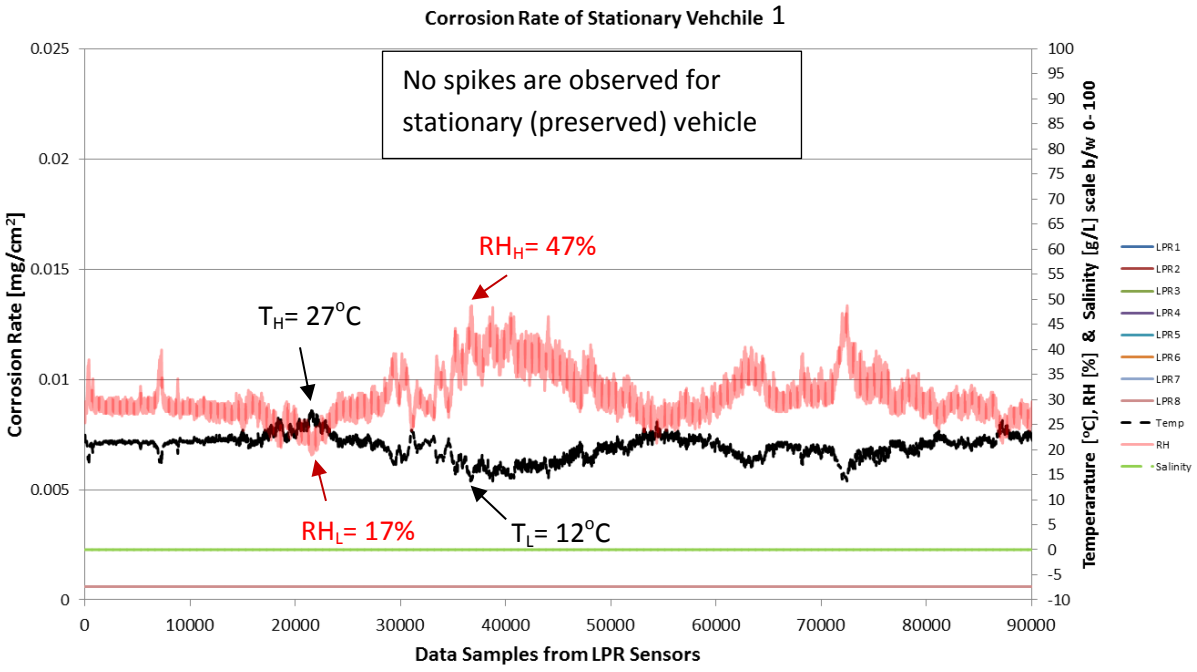

Figure 12. The long-term three years atmospheric corrosion rate data from stationary (preserved) vehicle corresponding to the change of temperature, relative humidity and condensate's salinity.

5. Comparison between an operating and a stationary vehicle

Following key parameters identify the main differences between an operating and a stationary vehicle in context of corrosion rate.

- ***Spikes in graphs:*** Operating vehicle was subjected to uncontrolled environmental conditions by numerous operations outside the tank museum. These operations were observed as several 'spikes' A to H in relative humidity, temperature and salinity graphs as shown in fig. 7. Each spike represented the sudden change in the above three parameters due to movement from indoor controlled to outdoor uncontrolled conditions. However, in the case of stationary vehicle which was constantly preserved inside the Tank Museum, no spikes were observed at all, as per expectations.

- ***Relative Humidity and Temperature:*** When the operating vehicle was operated from controlled to uncontrolled environment, the relative humidity increased due to corresponding decrease in controlled

temperature. This high relative humidity resulted in the formation of thin film of moisture on the surface of bare steel strictly considering the condition that relative humidity exceeded the critical relative humidity of steel. In the case of stationary vehicle this condition was never met.

- ***Critical Relative Humidity of Steel and Salinity:*** As the operating vehicle made certain indoor and outdoor trips, it started accumulating environmental pollutants on its unprotected steel parts. The accumulation of these hygroscopic salts resulted in the lower critical relative humidity of steel. During the operation of vehicle in the coastal region near the Museum it was observed that the critical value had gone as low as 20 %, due to high salinity value in addition to low temperature. Therefore when the vehicle was subjected to outdoor high relative humidity conditions, the corrosion started at early stage. In the case of stationary vehicle, there was no accumulation of hygroscopic salts on its unprotected parts and the corresponding critical relative humidity level of steel was high compared to the atmospheric relative humidity.

- ***TOW:*** In the case of operating vehicle, the first operation A had a low value of TOW, because the critical relative humidity of steel was high due to no/or very less contamination of steel surface as shown in fig. 9. As a result, the average corrosion rate was low in this first operation A. However, further operations resulted in stable TOW and corrosion rate after their subsequent decrease. In the case of stationary vehicle, TOW did not occur, because relative humidity never exceeded the critical relative humidity of steel.

6. Conclusions

Following conclusions were made from the 3 years μ LPR based comparative analysis of two set of large vehicles (operating and stationary):

1) The accumulation of hygroscopic salts contaminants on the exposed steel surface speeds-up the corrosion rate of steel under the low temperature and high relative humidity conditions. The exposed surface includes all those areas where coating has already delaminated. The corrosion in such delaminated areas accelerates the delamination rate leading to more area getting exposed until a complete coating failure has occurred. Therefore, to avoid coating failure as a result of corrosion it is better to treat such delaminated areas by proper repainting prior to exposure in uncontrolled environment.

2) The hygroscopic salts accumulated on the bare steel also reduce the critical relative humidity of steel to a considerable low level. This lower level leads to the formation of thin electrolytic film on the steel surface even at a very low value of atmospheric relative humidity which in turn initiates the corrosion process at early stage. Therefore, to avoid such early initiation, it is better to keep the exposed steel areas clean, also those including the delaminated areas.

3) The lower value of critical relative humidity of steel results in the larger TOW. This means that in such case the duration for which the steel surface will remain wet will increase providing more time for the corrosion reactions and hence resulting in large corrosion rate. Therefore, for ensuring the lower value of TOW, the steel surface in addition to cleaning factor must be applied with such organic compounds which can greatly reduce the wettability of steel surface.

4) TOW is a complex parameter which in addition to critical relative humidity of steel also depends on other physical parameters such as surface roughness, surface defects, position and orientation of exposed steel surface. These physical factors play an essential role in determining the wettability aspect of steel. Therefore it is equally important to consider the effect of these parameters while dealing with the corrosion problem of large steel structures.

5) The current research deployed uLPRs with a data acquisition strength in one meter diameter surface area. A total of 8 sensors suite was used for one large vehicle which covers majority of the surface area of the vehcile. The major objective was to investigate critical points in specific areas of large military tanks within

the museum, namely turret, armour plate, cockpit, near interacting joints and irregular geometrical surfaces. This installation was focused in terms of strategic points rather than the overall surface area. Modelling techniques have been developed [23] to extrapolate corrosion monitoring & prediction in less critical areas

Acknowledgements

The authors would like to acknowledge in-kind support provided by Defence Science and Technology Laboratory (DSTL) - Ministry of Defence (Professor Keith Stokes) and The Tank Museum Bovington UK (Mike Hayton and Richard Smith). Authors would also like to thank Paola Barbuto, Stephen Fordham and Dr Dean Bernard at SciTech Bournemouth University for supporting surface analyses and measurement techniques.

References

[1] K. E. Trenberth, A. Dai, R. M. Rasmussen, and D. B. Parsons, "The changing character of precipitation," *Bulletin of the American Meteorological Society*, vol. 84, pp. 1205-1217, 2003.

[2] T. Tsuru, K.-I. Tamiya, and A. Nishikata, "Formation and growth of micro-droplets during the initial stage of atmospheric corrosion," *Electrochimica Acta*, vol. 49, pp. 2709-2715, 2004.

[3] M. Morcillo, B. Chico, I. Díaz, H. Cano, and D. De la Fuente, "Atmospheric corrosion data of weathering steels. A review," *Corrosion Science*, vol. 77, pp. 6-24, 2013.

[4] A. P. Yadav, A. Nishikata, and T. Tsuru, "Electrochemical impedance study on galvanized steel corrosion under cyclic wet–dry conditions—influence of time of wetness," *Corrosion Science*, vol. 46, pp. 169-181, 2004.

[5] A. Saeed, Khan, Z., and Montgomery, E., "Corrosion Damage Analysis and material Characterization of Sherman and Centaur - The Historic Military Tanks," *Materials Performance and Characterization*, vol. 2, pp. 30-44, February 6, 2013.

[6] A. Saeed, Z. A. Khan, M. Hadfield, and S. Davies, "Material characterization and real-time wear evaluation of pistons and cylinder liners of the tiger 131 military tank," *Tribology Transactions*, vol. 56, pp. 637-644, // 2013.

[7] M. H. Nazir, Z. A. Khan, A. Saeed, and K. Stokes, "A model for cathodic blister growth in coating degradation using mesomechanics approach," *Materials and Corrosion*, 2015.

[8] M. H. Nazir, Z. A. Khan, A. Saeed, and K. Stokes, "Modeling the Effect of Residual and Diffusion-Induced Stresses on Corrosion at the Interface of Coating and Substrate," *Corrosion*, vol. 72, pp. 500-517, 2016/04/01 2015.

[9] A. Saeed, Z. Khan, M. Clark, N. Nel, and R. Smith, "Non-destructive material characterisation and material loss evaluation in large historic military vehicles," *Insight: Non-Destructive Testing and Condition Monitoring*, vol. 53, pp. 382-386, 2011.

[10] M. H. Nazir, Z. A. Khan, A. Saeed, and K. Stokes, "A predictive model for life assessment of automotive exhaust mufflers subject to internal corrosion failure due to exhaust gas condensation," *Engineering Failure Analysis*, vol. 63, pp. 43-60, 2016.

[11] A. Saeed, "Sustainable methodology of conserving historic military vehicles," Bournemouth University, 2013.

[12] A. Saeed, Z. A. Khan, and M. H. Nazir, "Time dependent surface corrosion analysis and modelling of automotive steel under a simplistic model of variations in environmental parameters," *Materials Chemistry and Physics*, vol. 178, pp. 65-73, 8/1/ 2016.

[13] M. H. Nazir, Z. A. Khan, and K. Stokes, "A holistic mathematical modelling and simulation for cathodic delamination mechanism – a novel and an efficient approach," *Journal of Adhesion Science and Technology*, pp. 1-39, 2015.

[14] Z. A. Khan, M. Grover, and M. H. Nazir, "The Implications of Wet and Dry Turning on the Surface Quality of EN8 Steel," in *Transactions on Engineering Technologies*, ed: Springer, 2015, pp. 413-423.

[15] M. H. Nazir, Z. Khan, and K. Stokes, "Modelling of metal-coating delamination incorporating variable environmental parameters," *Journal of Adhesion Science and Technology*, vol. 29, pp. 392-423, 2014.

[16] M. Nazir, Z. Khan, A. Saeed, and K. Stokes, "Modelling the Effect of Residual and Diffusion induced Stresses on Corrosion at the Interface of Coating and Substrate," *Corrosion*, 2015.

[17] M. H. Nazir, Z. A. Khan, and K. Stokes, "Optimisation of Interface Roughness and Coating Thickness to Maximise Coating-Substrate Adhesion - A Failure Prediction and Reliability Assessment Modelling," *Journal of Adhesion Science and Technology*, vol. 29, pp. 1415-1445, 2015.

[18] M. Nazir, Z. A. Khan, and K. Stokes, "A unified mathematical modelling and simulation for cathodic blistering mechanism incorporating diffusion and fracture mechanics concepts," *Journal of Adhesion Science and Technology*, vol. 29, pp. 1200-1228, 2015.

[19] M. H. Nazir, Z. A. Khan, and K. Stokes, "Analysing the coupled effects of compressive and diffusion induced stresses on the nucleation and propagation of circular coating blisters in the presence of micro-cracks," *Engineering Failure Analysis*, vol. 70, pp. 1-15, 2016.

[20] A. Saeed, Z. Khan, M. Clark, M. Nel, and R. Smith, "Non-destructive material characterisation and material loss evaluation in large historic military vehicles," *Insight-Non-Destructive Testing and Condition Monitoring*, vol. 53, pp. 382-386, 2011.

[21] M. H. Nazir, A. Saeed, and Z. Khan, "A comprehensive predictive corrosion model incorporating varying environmental gas pollutants applied to wider steel applications," *Materials Chemistry and Physics*, vol. 193, pp. 19-34, 2017.

[22] A. Saeed, Z. A. Khan, H. Nazir, M. Hadfield, and R. Smith, "Research Impact of Conserving Large Military Vehicles through a Sustainable Methodology," *International Journal of Heritage Architecture*, vol. 1, pp. 267-274, 2017.

[23] M. Nazir and Z. Khan, "A review of theoretical analysis techniques for cracking and corrosive degradation of film-substrate systems," *Engineering Failure Analysis*, 2016.

[24] R. Bajwa, Z. Khan, H. Nazir, V. Chacko, and A. Saeed, "Wear and Friction Properties of Electrodeposited Ni-Based Coatings Subject to Nano-enhanced Lubricant and Composite Coating," *Acta Metallurgica Sinica (English Letters)*, vol. 29, pp. 902-910, 2016.

[25] Z. A. Khan, P. Pashaei, R. Bajwa, H. Nazir, and M. Cakmak, "Fabrication and characterisation of electrodeposited and magnertron-sputtered thin films," *International Journal of Computational Methods & Experimental Measurements*, vol. 3, pp. 165-174, 2015.

[26] M. H. Nazir and Z. Khan, "Maximising the interfacial toughness of thin coatings and substrate through optimisation of defined parameters," *International Journal of Computational Methods and Experimental Measurements*, vol. 3, pp. 316-328, 2015.

[27] R. S. Bajwa, Z. Khan, V. Bakolas, and W. Braun, "Effect of bath ionic strength on adhesion and tribological properties of pure nickel and Ni-based nanocomposite coatings," *Journal of Adhesion Science and Technology*, vol. 30, pp. 653-665, 2016.

[28] R. S. Bajwa, Z. Khan, V. Bakolas, and W. Braun, "Water-Lubricated Ni-Based Composite (Ni–Al2O3, Ni–SiC and Ni–ZrO2) Thin Film Coatings for Industrial Applications," *Acta Metallurgica Sinica (English Letters)*, vol. 29, pp. 8-16, 2015.

[29] Linear Polarization Resistance (LPR) General Information "http://www.caproco.com/catalog/pdf/Probes-Instruments/Linear-Polarization-Resistance/LPR-General-Information.pdf" Retrieved on 11/07/2017

[30] "uLPR corrosion sensors developed by Analatom," *http://www.analatom.com/products-LPR.html; Retrieved on 14/05/2017*

[31] D. Brown, D. Darr, J. Morse, and B. Laskowski, "Real-time corrosion monitoring of aircraft structures with prognostic applications," in *Proceedings of the Annual Conference of the Prognostics and Health Management Society, Minneapolis, MN, USA*, 2012, pp. 23-27.

[32] D. Brown, D. Darr, J. Morse, and B. Laskowski, "Theoretical and experimental evaluation of a real-time corrosion monitoring system for measuring pitting in aircraft structures," in *Proceedings of the First European Conference of the Prognostics and Health Management Society, Dresden, Germany*, 2012, pp. 3-5.

[33] D. Brown, D. Darr, J. Morse, R. Betti, and B. Laskowski, "Advanced sensing, degradation detection, diagnostic and prognostic capabilities for structural health management," in *SPIE Smart Structures and Materials+ Nondestructive Evaluation and Health Monitoring*, 2012, pp. 83470G-83470G-11.

[34] D. BROWN, D. DARR, J. MORSE, B. LASKOWSKI, and R. BETTI, "Experimental Validation of a Micro-Sized Polarization Resistance Corrosion Sensor for Structural Health Management Applications."

[35] D. W. Brown, R. J. Connolly, D. R. Darr, and B. Laskowski, "Linear Polarization Resistance Sensor Using the Structure as a Working Electrode," *PHM Society, EUROPEAN CONFERENCE OF THE PROGNOSTICS AND HEALTH MANAGEMENT SOCIETY 2014*, vol. 5, pp. 1-7, 2014.

[36] R. J. Connolly, D. Brown, D. Darr, J. Morse, and B. Laskowski, "Corrosion Detection on Buried Transmission Pipelines with Micro-Linear Polarization Resistance Sensors," in *Engineering Asset Management - Systems, Professional Practices and Certification: Proceedings of the 8th World Congress on Engineering Asset Management (WCEAM 2013) & the 3rd International Conference on Utility Management & Safety (ICUMAS)*, P. W. Tse, J. Mathew, K. Wong, R. Lam, and C. N. Ko, Eds., ed Cham: Springer International Publishing, 2015, pp. 673-685.

[37] F. Mansfeld, "The polarization resistance technique for measuring corrosion currents," in *Advances in corrosion science and technology*, ed: Springer, 1976, pp. 163-262.

[38] J. R. Scully, "Polarization resistance method for determination of instantaneous corrosion rates," *Corrosion*, vol. 56, pp. 199-218, 2000.

[39] D. Brown, D. Darr, J. Morse, and B. Laskowski, "Theoretical and Experimental Evaluation of a Real-Time Corrosion Monitoring System for Measuring Pitting in Aircraft Structures," *First European Conference of the Prognostics and Health Management Society 2012*, vol. 3, pp. 1-9, 2012.

[40] V. Feliu, J. González, C. Adrade, and S. Feliu, "Equivalent circuit for modelling the steel-concrete interface. II. Complications in applying the stern-geary equation to corrosion rate determinations," *Corrosion science*, vol. 40, pp. 995-1006, 1998.

[41] D. W. Brown, R. J. Connolly, B. Laskowski, M. Garvan, H. Li, V. S. Agarwala, and G. Vachtsevanos, "A Novel Linear Polarization Resistance Corrosion Sensing Methodology for Aircraft Structure."
[42] N. A. Weather Underground. (2011, *http://www.wunderground.com/weatherstation/WXDailyHistory.asp?ID=IDORSETB5*.
[43] "GOOGLE MAPS, 2016. Map of THE TANK MUSEUM BOVINGTON UK. [online]. Google. Available from: https://www.google.co.uk/maps/place/The+Tank+Museum/@50.6943613,-2.2434328,15z/data=!4m5!3m4!1s0x0:0x3b0785b71b79cf5b!8m2!3d50.6943613!4d-2.2434328."
[44] "Battle tank Images taken from FPRADO online: http://www.fprado.com/armorsite/abrams.htm; Last updated: 23/11/2016."